Function and solution structure of hainantoxin-I, a novel insect sodium channel inhibitor from the Chinese bird spider *Selenocosmia hainana*[1]

Dongling Li[a], Yucheng Xiao[b], Weijun Hu[b], Jinyun Xie[b], Frank Bosmans[c], Jan Tytgat[c], Songping Liang[b,*]

[a]*College of Life Sciences, Peking University, Beijing 100871, PR China*
[b]*College of Life Sciences, Hunan Normal University, Changsha 410081, PR China*
[c]*Laboratory of Toxicology, University of Leuven, E. Van Evenstraat 4, 3000 Leuven, Belgium*

Abstract Hainantoxin-I is a novel peptide toxin, purified from the venom of the Chinese bird spider *Selenocosmia hainana* (= *Ornithoctonus hainana*). It includes 33 amino acid residues with a disulfide linkage of I–IV, II–V and III–VI, assigned by partial reduction and sequence analysis. Under two-electrode voltage-clamp conditions, hainantoxin-I can block $rNa_v1.2/\beta_1$ and the insect sodium channel para/tipE expressed in *Xenopus laevis* oocytes with IC_{50} values of 68 ± 6 μM and 4.3 ± 0.3 μM respectively. The three-dimensional solution structure of hainantoxin-I belongs to the inhibitor cystine knot structural family determined by two-dimensional ^1H nuclear magnetic resonance techniques. Structural comparison of hainantoxin-I with those of other toxins suggests that the combination of the charged residues and a vicinal hydrophobic patch should be responsible for ligand binding. This is the first report of an insect sodium channel blocker from spider venom and it provides useful information for the structure–function relationship studies of insect sodium channels.
© 2003 Published by Elsevier B.V. on behalf of the Federation of European Biochemical Societies.

Key words: Hainantoxin-i; Neurotoxin; Sodium channel; Solution structure; ICK motif

1. Introduction

Voltage-gated sodium channels (VGSCs) are major contributors to the initiation and propagation of the action potentials in excitable cells. They are composed of a functional pore-forming α subunit (260 kDa) associated with up to three auxiliary β subunits (21–23 kDa) [1,2]. To date nine mammalian ($Na_v1.1$–$Na_v1.9$) and three invertebrate VGSC subtypes have been cloned, functionally expressed and characterized. With more than 75% sequence identity with one another, these subtypes show relatively similar pharmacological properties in different expression systems, although their response to certain ligands can be quite different [3,4].

VGSCs have been highly conserved during evolution [5]. Although the receptor sites have been predominantly identified and characterized by vertebrate preparations, binding experiments indicate that insect neuronal VGSCs possess similar receptor sites [6]. However, there are also differences between the two classes of VGSCs. Compared with vertebrate VGSCs, insect VGSCs are generally more sensitive to tetrodotoxin (TTX). Furthermore, some ω-toxins (e.g. ω-conotoxin MVIIC and ω-agatoxin IVA) fail to target mammal Na^+ channels, but block TTX-sensitive (TTX-S) Na^+ currents in insect membranes [7]. To date, more than six neuronal receptor sites on VGSCs have been identified to bind toxins [8].

Spider venoms contain a variety of toxins that target voltage-gated ion channels and have been used as a potential source of new compounds with specific pharmacological properties. According to their functional characteristics on VGSCs, the 27 spider peptides or homologues from the PubMed database (www.pubmed.com) can be divided into two groups: depressant and excitatory toxins. Depressant toxins (e.g. HNTX-IV and HWTX-IV) specifically inhibit the mammal neuronal TTX-S VGSCs through a mechanism quite similar to that of TTX without affecting the activation or inactivation kinetics [9,10]. Excitatory toxins (e.g. μ-agatoxins and δ-atracotoxins), acting at site 3 on the vertebrate and/or insect VGSCs, inhibit the inactivation in a similar manner to α-scorpion toxins and ATXII [11,12]. Among these site 3 toxins, some specifically activate insect VGSCs (e.g. μ-agatoxins I and IV, curtatoxins I–III) [11,12]; several target both mammalian and insect VGSCs (e.g. δ-ACTX-Ar1 and δ-ACTX-Hv1a) [13] and others show no effect on insect VGSCs (e.g. δ-ACTX-HV1b) [14]. Radio-ligand binding experiments reveal that these site 3 toxins compete with [^{125}I]Lqh II or [^{125}I]LqhαIT, two well-defined ligands of receptor site 3, in both rat brain and cockroach neuronal membranes. They are extremely potent and define a new class of toxins affecting both insect and mammalian VGSCs [15,16].

The Chinese bird spider *Selenocosmia hainana* (= *Ornithoctonus hainana*) is distributed in the hilly areas of Hainan province in southern China [17]. Its crude venom can inhibit TTX-S Na^+ currents induced on neuroblastoma × glioma hybrid (NG108-15) cells with the IC_{50} value of 1.8 mg/l [18].

*Corresponding author. Fax: (86)-731-8861304.
E-mail address:* liangsp@hunnu.edu.cn (S. Liang).

Hainantoxin-I (HNTX-I) is the most abundant component in the crude venom, but previous patch-clamp experiments indicated that HNTX-I failed to affect the normal activities of TTX-S VGSCs, voltage-gated delay-rectified outward potassium channels and voltage-gated calcium channel on NG108-15 cells [18]. In the present study, we report the characterization of HNTX-I inhibiting the TTX-S insect VGSC para/tipE and $rNa_v1.2/\beta_1$ channel expressed in *Xenopus laevis* oocytes, the determination of its disulfide linkage, and the solution structure determined using 2D ^1H nuclear magnetic resonance (NMR) spectroscopy as a typical inhibitor cystine knot (ICK) motif [19]. Furthermore, a detailed comparison of the structure of HNTX-I and other previously known toxins targeting ion channels provides a basis for deducing the structure–function relationships for these molecules and their interaction with potential target receptors.

2. Materials and methods

2.1. Toxin purification and sequencing

The venom from adult female *O. hainana* spiders was collected and purified by ion-exchange chromatography and reversed-phase high performance liquid chromatography (RP-HPLC) as described in our previous work [9]. The molecular mass was determined by matrix-assisted laser desorption/ionization time-of-flight (MALDI-TOF) mass spectrometry on a Voyager-DE™ STR Biospectrometry™ workstation. The entire amino acid sequence was obtained from a single sequencing run on an Applied Biosystems/Perkin-Elmer Life Sciences Procise 491-A protein sequencer.

2.2. Assignment of the disulfide bonds of HNTX-I

To determine the specific disulfide connections of HNTX-I, partial reduction by Tris (2-carboxyethyl)phosphine (TCEP) at low pH was employed [9]. 0.1 mg HNTX-I, dissolved in 10 μl of 0.1 M citrate buffer (pH 3) containing 6 M guanidine-HCl, was partially reduced by adding 10 μl of 0.1 M TCEP at 40°C for 10 min at pH 3. The intermediates were isolated by RP-HPLC and their masses were determined by MALDI-TOF mass spectrometry. Appropriate intermediates containing free thiols were dried and then alkylated by adding 100 μl of 0.5 M iodoacetamide (pH 8.3). The alkylated peptide was desalted by RP-HPLC and then submitted to an Applied Biosystems 491-A protein sequencer.

2.3. Expression in X. laevis oocytes

For the expression in *X. laevis* oocytes, the para/pGH19-13-5 vector [20], tipE/pGH19 vector [21,22] and rBrainII(Na$_v$1.2)/pLCT1 vector [23] were linearized with *Not*I and transcribed with the T7 mMES-SAGE-mMACHINE kit (Ambion, USA). The β_1 gene was subcloned into pSP64T [24]. For in vitro transcription, β_1/pSP64T was first linearized with *Eco*RI. Next, capped cRNA was synthesized from the linearized plasmid using the large-scale SP6 mMESSAGE-mMACHINE transcription kit (Ambion).

The harvesting of oocytes from anesthetized female *X. laevis* frogs was as previously described [25]. Oocytes were injected with 50 nl of cRNA at a concentration of 1 ng/nl using a Drummond micro-injector (USA). The ND96 solution used for incubating the oocytes contained (in mM): NaCl 96, KCl 2, CaCl$_2$ 1.8, MgCl$_2$ 2 and HEPES 5 (pH 7.4), supplemented with 50 mg/l gentamicin sulfate. HNTX-I powder was dissolved in ND96 containing 0.1% bovine serum albumin.

2.4. Electrophysiological recordings in Xenopus oocytes

Two-electrode voltage-clamp recordings were performed at room temperature (18–22°C) using a GeneClamp 500 amplifier (Axon Instruments, USA) controlled by a pClamp data acquisition system (Axon Instruments). Whole-cell currents from oocytes were recorded 3–4 days after injection. Voltage and current electrodes were filled with 3 M KCl. Resistances of both electrodes were kept as low as possible (< 0.5 MΩ). Bath solution composition was (in mM): NaCl 96, KCl 2, CaCl$_2$ 1.8, MgCl$_2$ 2 and HEPES 5 (pH 7.4). Using a four-pole low-pass Bessel filter, currents were filtered at 2 kHz and sampled

at 10 kHz. Leak and capacitance subtraction were performed using a P/4 protocol. Current traces were evoked in an oocyte expressing the cloned VGSCs by depolarizations between −70 and 40 mV, using 10 mV increments, from a holding potential of −90 mV. Curve manipulations were performed using pClamp8 (Axon Instruments) and Origin software (Microcal, USA).

2.5. NMR spectroscopy

NMR samples were prepared by dissolving the native HNTX-I in 500 μl of 20 mM deuterium sodium acetate buffer (H$_2$O/D$_2$O, 9/1, v/v) with a final concentration of 4.5 mM (pH 4.0). All NMR spectra were observed on a 500 MHz Bruker DRX-500 spectrometer with a sample temperature of 298 K. The hydrogen–deuterium exchange experiments were carried out by recording a series of 1D spectra after the lyophilized sample was redissolved in D$_2$O. Several sets of 2D spectra were recorded in a phase-sensitive mode by the time-proportional phase incrementation method following standard pulse sequences and phase cycling. Solvent suppression was achieved by the presaturation method. Total correlated spectroscopy spectra were obtained with a mixing time of 100 ms. Nuclear Overhauser effect spectroscopy (NOESY) spectra were recorded with a mixing time of 200 ms in D$_2$O and of 100, 200 and 400 ms in H$_2$O. All spectra were processed and analyzed using Felix 98.0 software (Biosym Technologies) running on a Silicon Graphics O2 workstation.

2.6. Structure calculations

Distance constraints were obtained from the intensities of cross-peaks in NOESY spectra with a mixing time of 200 ms. All NOE data were classified into four distance ranges, 1.8–2.7 Å, 1.8–3.5 Å, 1.8–5.0, 1.8–6.0 Å, corresponding to strong, medium, weak and very weak NOE values, respectively. Pseudo-atom corrections were applied to non-stereospecifically assigned methyl and methylene protons according to the method of Wüthrich [26]. Ten ϕ dihedral angle restraints derived from $^3J_{NH-C\alpha H}$ coupling constants were restrained to $-120 \pm 30°$ for $^3J_{NH-C\alpha H} \geq 8.80$ Hz and $-120 \pm 40°$ for $8.00 \leq$ $^3J_{NH-C\alpha H} < 8.80$ Hz. Three distance constraints were added to every disulfide bond. The corresponding distances were 2.02 ± 0.02 Å, 2.99 ± 0.5 Å, and 2.99 ± 0.5 Å for S(i)–S(j), S(i)–C$_\beta$(j), and S(j)–C$_\beta$(i), respectively. Ten hydrogen bond constraints confined the NH(i)–O(j) and N(i)–O(j) distances as 1.8–2.3 Å and 2.8–3.3 Å, respectively, according to slowly exchanging amide protons and NOE patterns. Structure calculations of HNTX-I were run on a Silicon Graphics workstation using the standard protocol of the X-PLOR 3.851 program [27].

3. Results

3.1. Isolation and sequencing of HNTX-I

HNTX-I was purified by a combined use of ion-exchange HPLC and RP-HPLC as described before [9] (Fig. 1). The amino acid sequence of HNTX-I determined by Edman degradation, as shown in Fig. 2, consists of 33 amino acid residues including six Cys residues. Its experimental average molecular mass is 3608.02 Da and monoisotopic molecular mass is 3605.62 Da, consistent with the calculated molecular mass for HNTX-I-amide. Hence, it was concluded that HNTX-I is C-terminally amidated. The amino acid sequence of HNTX-I reported here redressed the incorrect four residues at the C-terminus of the first reported sequence of HNTX-I [18]. The final sequence of this toxin has been confirmed by the data of disulfide bond assignment and the 2D-NMR experiment in this study.

3.2. Assignment of the disulfide bonds of HNTX-I

Reduction of HNTX-I by TCEP led to the isolation of three partially reduced peptides (Fig. 3, peaks I, IIa and IIb), determined by MALDI-TOF mass spectrometry analysis. The three peaks were collected and alkylated rapidly with iodoacetamide following purification by analytical RP-HPLC.
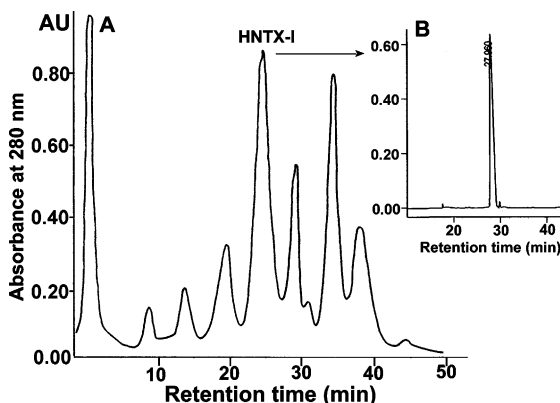
Fig. 1. Purification of HNTX-I. A: Ion-exchange HPLC profile of crude *O. hainana* venom (the elution site of HNTX-I is labelled). Lyophilized venom was applied to a Waters Protein-Pa™ CM 15HR ion-exchange column (10×100 mm). Buffer A: 0.1 M NaH_2PO_4; buffer B: 0.1 M Na_2HPO_4; buffer C: 1 M NaCl; buffer D: ddH_2O; flow rate, 3.0 ml/min; gradient: A 8%, B 2%, C 0–90% 0–50 min; wavelength detector: 280 nm. B: Analytical RP-HPLC profile of HNTX-I. The peak labeled with HNTX-I in ion-exchange chromatography was applied to a Vydac C18 column (4.6×250 mm). Elution was performed with a linear gradient of 15–45% acetonitrile/0.1% trifluoroacetic acid in ddH_2O for 45 min at a flow rate of 0.7 ml/min.

Molecular weight determination and sequencing indicated that the free thiols of these three peptides had been alkylated.

In Fig. 4A, Pth-CM-Cys signals were observed in the chromatograms at the 2nd and 17th cycles when sequencing alkylated peak I, while no signals were observed at the remaining cysteine cycles. The result indicates that the only reduced disulfide bond is Cys2–Cys17. When sequencing alkylated peak IIa, Pth-CM-Cys signals were observed at the 2nd, 9th, 17th and 22nd cycles (Fig. 4B), indicating that Cys16 is still linked to Cys29 by a disulfide bond. For alkylated peak IIb, Pth-CM-Cys signals were observed at the 2nd, 16th, 17th, and 29th sequencing cycles (Fig. 4C), suggesting that the remaining disulfide bond is Cys9–Cys22. Accordingly, the disulfide linkage of HNTX-I was determined to be Cys2–Cys17, Cys9–Cys22 and Cys16–Cys29. This disulfide pattern (I–IV, II–V and III–VI) is frequently found in a variety of toxic and inhibitory polypeptides from biologically diverse sources.

Fig. 2. Comparison of the amino acid sequence of HNTX-I with HWTX-I and previously described VGSC blockers from the venom of the Chinese bird spider *Ornithoctonus*. ☆ represents an amidated C-terminus. # shows the sequence of HNTX-III from the SwissProt knowledgebase under accession number P83464. ✳ shows the extremely well conserved residues important for their functions. Identical residues and conservatively substituted residues are shaded in black and gray, respectively. The disulfide bridge pattern of these toxins is indicated above the sequences. HWTX-I is an N-type Ca^{2+} channel blocker [38]. HWTX-IV, HNTX-III–V block TTX-S VGSCs expressed in adult rat dorsal root ganglion neurons [9,10,30]. HNTX-I blocks $rNa_v1.2/\beta_1$ and para/tipE expressed in *X. laevis* oocytes.
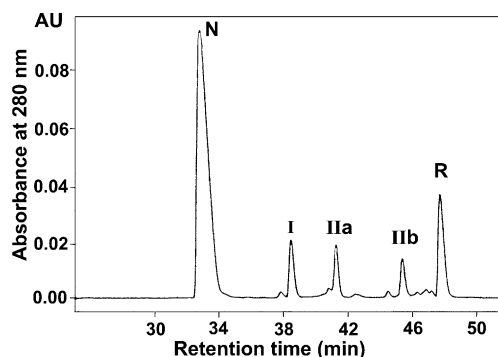

Fig. 3. Analytical RP-HPLC profile of partial reduction of HNTX-I by TCEP. The five chromatographic peaks contain intact peptide and partially reduced intermediates, respectively. The main peak (peak N) represents intact HNTX-I, whose observed mass is the same as the native HNTX-I. Peak I with a mass 2 Da greater than that of native peptide indicates one of the three disulfide bonds possibly reduced. The masses of peaks IIa and IIb are both 4 Da heavier than the native HNTX-I, suggesting that two disulfide bonds are reduced to four free thiol groups. Peak R represents completely reduced peptide with a mass 6 Da heavier than the intact peptide.

3.3. Effects of HNTX-I on sodium channel currents

Using the two-electrode voltage-clamp technique on *X. laevis* oocytes, a pharmacological comparison was made regarding the effects of HNTX-I on two different cloned sodium channels. Current traces were evoked using 25 ms step depolarizations to a voltage range between −70 and 40 mV depending on the sodium channel, from a holding potential of −90 mV. The effect of HNTX-I on a TTX-S vertebrate neuronal VGSC ($Na_v1.2$ from rat co-expressed with the vertebrate
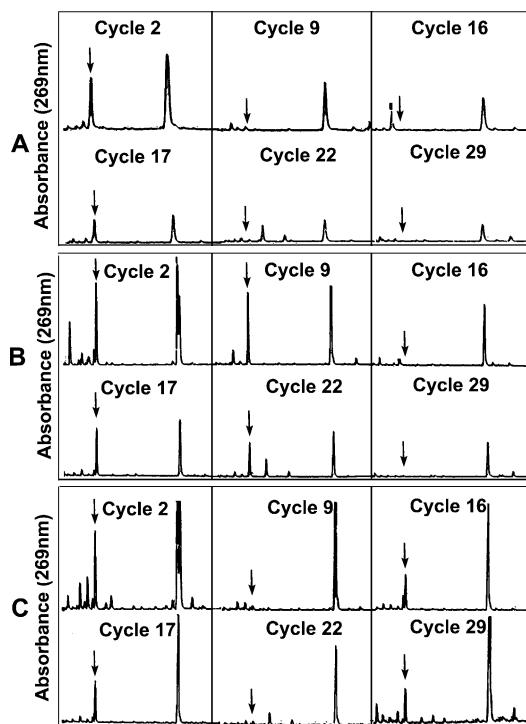

Fig. 4. RP-HPLC sequencing profile of partially reduced intermediates after modification with iodoacetamide. Cys residues occur at cycles 2, 9, 16, 17, 22 and 29. The elution position of Pth-CM-Cys is marked with arrows. A: The Cys residue cycles of alkylated peak I. B: The Cys residue cycles of alkylated peak IIa. C: The Cys residue cycles of alkylated peak IIb.
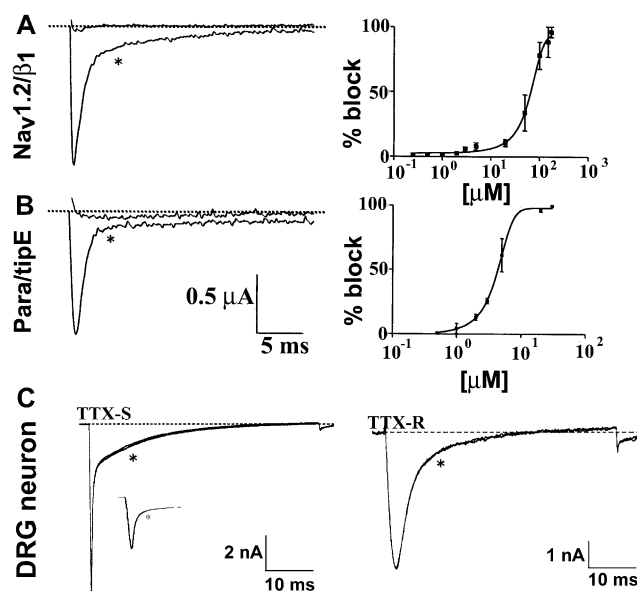
Fig. 5. Effects of HNTX-I on VGSCs. Current traces were evoked by depolarizations ranging from −10 to 0 mV depending on the sodium channel, from a holding potential of −90 mV. * represents control conditions where no toxin was added. A,B: Left column represents the maximum effects of HNTX-I obtained on para/tipE (addition of 20 μM) and Na$_v$1.2/β$_1$ (addition of 200 μM) expressed in *X. laevis* oocytes. Right column represents the comparison of their dose–response curves. A sodium current block was observed for both VGSCs. Data are mean ± S.E.M. of at least three experiments. IC$_{50}$ values are discussed in the text. C: Both TTX-S and TTX-R VGSCs were unaffected by 100 μM HNTX-I on dorsal root ganglion (DRG) neurons, isolated from adult rat by the method described in [9,10]. Internal solution in mM: CsF 135, NaCl 10, HEPES 5 at pH 7.0. External solution in mM: NaCl 30, CsCl 5, D-glucose 25, MgCl$_2$ 1, CaCl$_2$ 1.8, HEPES 5, tetraethylammonium chloride 20, tetramethylammonium chloride 70 at pH 7.4. 200 nM TTX was added to the external solution to separate TTX-R sodium currents from TTX-S sodium currents.

β$_1$ subunit) was compared to an insect neuronal VGSC (para from *Drosophila melanogaster* co-expressed with the insect tipE subunit). HNTX-I causes a block of 100% when applied to both VGSCs (Fig. 5). No shift in the *I–V* curve was observed (Fig. 6). Although active on both neuronal VGSCs, HNTX-I possesses higher potency on para/tipE (as shown in Fig. 5). The following IC$_{50}$ values were obtained after a sigmoidal fit of the data: para/tipE 4.3 ± 0.3 μM and Na$_v$1.2/β$_1$ 68 ± 6 μM. HNTX-I is more than 15-fold more potent on para/tipE as compared to Na$_v$1.2/β$_1$.

3.4. Structure calculations and evaluation

Sequence-specific resonance assignments were performed according to the standard method [26]. All of the backbone protons and more than 96% of the side chain protons were identified in our previous paper [28]. A total of 329 non-redundant distance constraints and 10 dihedral constraints were used for the final calculations of HNTX-I. A family of 20 accepted structures with lower energies and better Ramachandran plots were selected to represent the 3D solution structure of HNTX-I. The structures have no distance violations greater than 0.2 Å and no dihedral violations greater than 2.0°. Furthermore, they also have no serious contacts and no distortions, as shown by the low values of the mean Lennard–Jones potential and the small deviations from ideal bond lengths
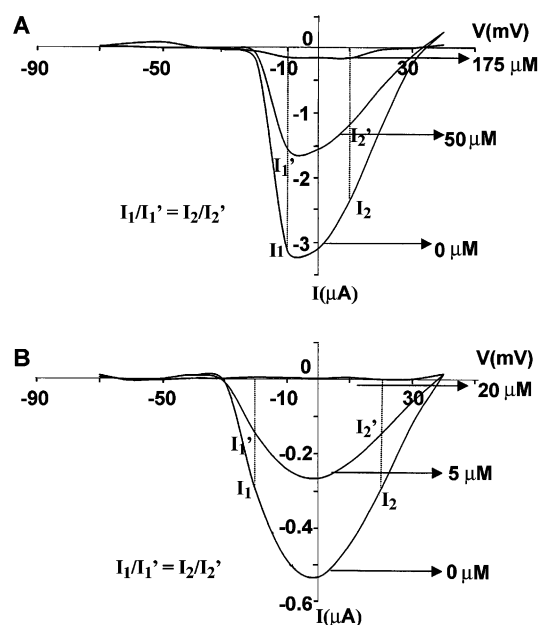

Fig. 6. *I–V* relationships of Na$_v$1.2/β$_1$ and para/tipE at different HNTX-I concentrations. The results of one oocyte are shown as an example. No shift in the *I–V* curve was observed ($I_1/I_1' = I_2/I_2'$). I_1, I_1', I_2 and I_2' are indicated in the figures. A: Na$_v$1.2/β$_1$. B: para/tipE.

Table 1
Structural statistics for 20 structures of HNTX-I

Parameter	Value
Experimental constraints	
Intra-residue NOE ($i–j = 0$)	155
Sequential NOE ($|i–j| = 1$)	99
Medium-range NOE ($|i–j| = 5$)	27
Long-range NOE ($|i–j| = 5$)	92
Dihedral angle (ϕ)	10
Average potential energies (kcal mol^{-1})[a]	
E_{total}	−46.90 ± 8.474
E_{bond}	5.10 ± 0.404
E_{angle}	39.15 ± 1.023
$E_{improper}$	4.388 ± 0.161
E_{vdW}	−95.84 ± 7.670
E_{NOE}	0.281 ± 0.169
E_{cdih}	0.021 ± 0.028
r.m.s. deviation from experimental constraints[b]	
NOE distance (Å) (392)	0.003 ± 0.001
Dihedral angle (°) (10)	0.138 ± 0.127
r.m.s. deviations from idealized geometry[a]	
Bonds (Å)	0.003 ± 0.0001
Angles (°)	0.536 ± 0.007
Impropers (°)	0.336 ± 0.005
Average r.m.s. differences versus mean structure (Å)	
Backbone atoms (N, Cα, C)	0.624 ± 0.073
Non-hydrogen heavy atoms	1.300 ± 0.130
Pairwise r.m.s. differences of 20 structures (Å)	
Backbone atoms (N, Cα, C)	0.902 ± 0.139
Non-hydrogen heavy atoms	1.848 ± 0.204

[a]The idealized geometry and energy values were defined by the CHARMM force field as implemented in the XPLOR program. All statistical values of energies, r.m.s. deviations, and r.m.s. differences are given as the mean ± S.D.
[b]The statistics of experimental r.m.s. deviation of NOE and dihedral angle constraints were from the calculation with force constants of 50 kcal/mol/Å^2 and 200 kcal/mol/rad^2, respectively.
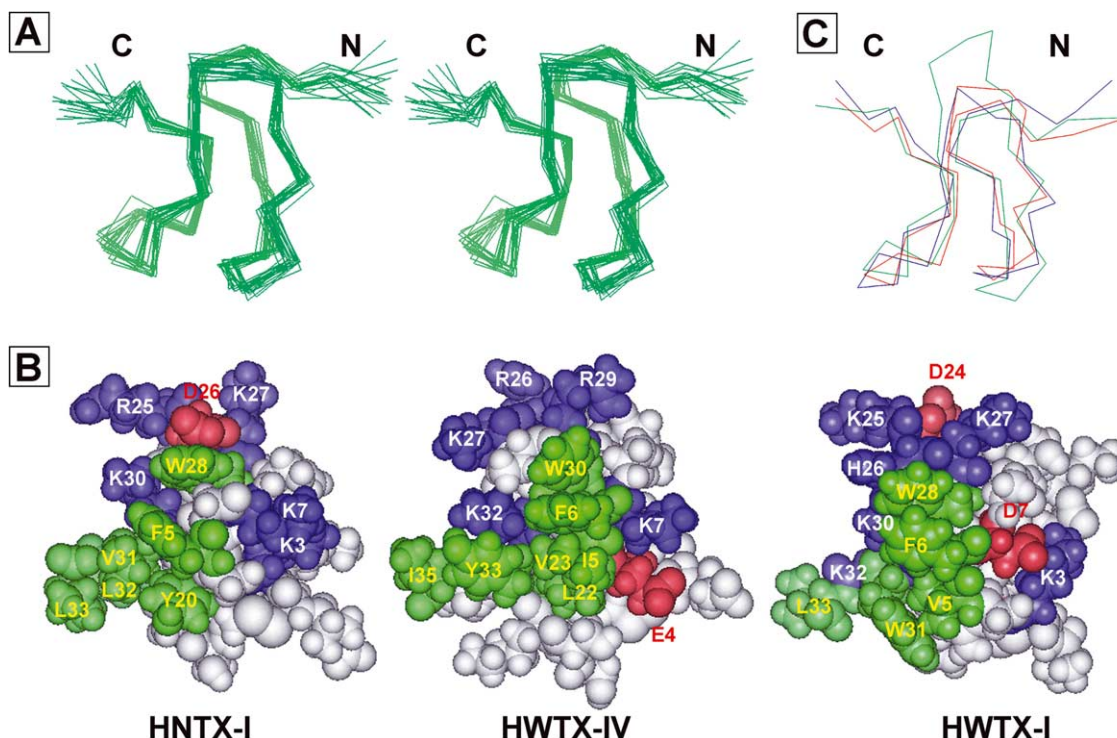
Fig. 7. Solution structure characterization of HNTX-I. A: Stereo view of superimposition of backbone heavy atoms (N, Cα, C) for 20 converged structures of HNTX-I. The letters N and C refer to the amino- and carboxy-termini, respectively. B: Comparison of the surface profile of HNTX-I (PDB code 1NIX), HWTX-IV (PDB code 1MB6) and HWTX-I (PDB code 1QK6). Blue and red regions represent positively and negatively charged residues, respectively. Green regions represent hydrophobic residues. C: Backbone superposition of HNTX-I (red), HWTX-I (blue) and HWTX-IV (green). The fit was done using the common secondary structure elements. (For interpretation of the references to color in this figure legend, the reader is referred to the web version of this article.)

and bond angles, respectively. Analysis of the structures in PROCHECK shows that 83.3% of non-Pro, non-Gly residues lie in the most favored regions of the Ramachandran plot. 16.7% are located in additionally allowed regions. A summary of the structural statistics for HNTX-I is given in Table 1.

3.5. Description of structures

Fig. 7A shows a stereo pair representation of the best-fit superposition of the backbone atoms (N, Cα, C) for the 20 converged structures of HNTX-I. Analysis of the 20 converged structures indicates that the molecular structure of HNTX-I contains a short triple-stranded anti-parallel β-sheet formed by the strands Lys7–Cys9, Tyr20–Asn23 and Trp28–Val31 respectively. The topology and constituting residues of the β-sheet, determined by calculations, were found to be in concordance with those determined by the analysis of secondary structures in our previous paper [28]. The turns in HNTX-I were also identified using a standard definition that states that the distance between Cα(i) and Cα(i+3) should be less than 7 Å and that the characteristic NOE connectivities of backbone protons [26] for the corresponding turn segments are present. These analyses led to the identification of four β-turns, which were classified according to Richardson [29]. The four β-turns involve residues Gly4–Lys7 (type II), Val10–Lys13 (type II), Cys17–Tyr20 (type II) and Ser24–Lys27 (type I).

The solution structure of HNTX-I shows a similar overall molecular fold to that adopted by numerous toxic and inhibitory peptides, which is called the ICK motif. The cysteine knot in HNTX-I is formed by three disulfide bonds linked

as Cys2–Cys17, Cys9–Cys22 and Cys16–Cys29, in which the Cys16–Cys29 disulfide bond passes through a 14-residue ring formed by the intervening polypeptide backbone and the Cys2–Cys17 and Cys9–Cys22 disulfide bonds.

4. Discussion

HNTX-I, isolated from the venom of *O. hainana*, is a novel depressant spider toxin preferentially blocking insect VGSCs. It neither slows channel inactivation nor shifts the reversal potential, indicating that it does not affect the ion selectivity of both VGSCs which were tested (Nav1.2/β1 and para/tipE). Compared with other depressant spider toxins such as HWTX-IV and HNTX-III–V [9,10,30], HNTX-I has no effect on the VGSC subtypes in dorsal root ganglion neurons containing rNav1.1, 1.6, 1.7, 1.8 and 1.9 (see Fig. 5C) nor on rNav1.4 and 1.5 expressed on *X. laevis* oocytes (data not shown), although none of them affected the activation and inactivation kinetics of sodium channels. HNTX-I can only target other channel isoforms, namely rNav1.2 and para/tipE channels, with IC50 values of 68±6 μM and 4.3±0.3 μM, respectively. It seems that similar to TTX and ATXII, HNTX-I is more potent on insect VGSCs than on their vertebrate counterparts [7]. Spider toxins targeting insect sodium channels emerge mainly in the excitatory toxins, such as δ-ACTXs and μ-agatoxins [11–13]. However, clearly different from these insect toxins, HNTX-I has no effect on the inactivation kinetics. The spider toxin HNTX-I reported here is the first to block insect sodium channels, and seems to be a site 1 toxin affecting the sodium channel through a mechanism quite

similar to that of TTX. Thus, it defines a new class of spider toxins affecting VGSCs, and could prove to be a novel useful ligand to investigate the multiple molecular forms of VGSCs in vertebrates as well as in insects.

4.1. Structure–function relationships of HNTX-I

Compared to other animal toxin groups, relatively little structural information has been gathered on spider peptide toxins affecting VGSCs. Up to now, six NMR solution structures (including HNTX-I) and one model structure have been deposited in the PDB (www.rcbs.org/pdb). Collectively, they all adopt the ICK structural motif. However, these peptides might possess a unique selectivity to mammals and/or insects VGSCs, distinct potencies and diverse receptor binding specificities. Of the structures deposited in the PDB, HNTX-I is the only one reported so far as being an insect inhibitor. Therefore, elucidation of the 3D structure of HNTX-I provides important clues on its toxin–receptor interaction.

In general, hydrophobic residue and polar residue hot spots are important binding determinants in protein interactions because of their conducting to energetically and structurally favorable states [31]. Studies of site-directed mutagenesis in VGSCs or their neurotoxins have also been carried out to identify which residues are involved in the binding and blocking activity [8,32–36]. One important characteristic required for blockage of sodium current is the presence of a positively charged region on the toxin since two important amino acids in the P loop form the negatively charged outer and inner rings that served as a receptor site for pore blockers and the selectively filter. The resultant electrostatic forces conduce to the attachment of the toxin to its binding site on the channel [37]. Since HNTX-I inhibits VGSCs in both vertebrates and insects, it should therefore present a similar type of interacting surface. Such a basic profile is also found in HNTX-I, in which there is relative abundance of Arg and Lys residues (Fig. 2), producing a net positive charge (theoretical $pI = 8.65$) on this molecule. The fact that the most solvent-exposed Arg and Lys residues of loop IV are extremely well conserved among the depressant spider toxins (Fig. 2) emphasizes the possibility that Arg25 and Lys27 in HNTX-I are the most crucial residues for its blocking activity. Close to the two residues are another basic residue Lys30, an acidic residue Asp26, and a hydrophobic patch (Phe5, Tyr20, Trp28, Val31, Leu32 and Leu33). Two other basic residues Lys3 and Lys7 are localized on the edge of the surface profile (Fig. 7B). The overall physicochemical characteristics of the proposed functional surface formed by all of the above mentioned amino acids are therefore in accord with those of ion channel inhibitors. From these data it is possible to conclude that the basic nature of HNTX-I is a crucial factor for its biological activity, and the surface of HNTX-I encompassing the charged residues and a vicinal hydrophobic patch is responsible for binding to VGSCs in both vertebrates and insects.

4.2. Structural comparisons of HNTX-I with HWTX-I and HWTX-IV

HNTX-I is closely related in primary sequence to other toxins from the venom of the Chinese bird spider *Ornithoctonus* (Fig. 2). Moreover, it shares a similar molecular folding to that of HWTX-I, an N-type Ca^{2+} channel inhibitor [38,39], and the mammal neuronal VGSC antagonist HWTX-IV [10]

(Fig. 6C). The sequence alignment and the structural comparison of these toxins indicate that the hydrophobic residues and most of the positively charged residues are fairly conserved. However, the distributions of negatively charged residues are obviously different (Fig. 7B). The residues corresponding to Lys3 and Asp26 of HNTX-I are Glu4 and Arg26 of HWTX-IV, respectively. The basic residue Lys7 in HNTX-I is changed into the acidic residue Asp7 in HWTX-I. A detailed analysis shows that Asp26 in HNTX-I and Asp24 in HWTX-I exhibit a slightly different location and orientation. Such subtle differences of charged residues do not alter the overall structure of the toxins but considerably affect their electrostatic properties and result in additional pharmacological flexibility. Based on our results, we propose that the conserved hydrophobic residue and positively charged residue hot spots of these toxins act as an ion channel binding site anchor, whereas the variable acidic residues and the local structure differences are considered to be responsible for their pharmacological specificity.

5. Conclusion

In summary, HNTX-I shows no effect on the neuronal TTX-S VGSCs in adult rat dorsal root ganglion neurons nor does it target VGSCs in cardiac or skeletal muscles of mammals. It selectively blocks $rNa_v1.2/\beta_1$ and para/tipE channels expressed in *X. laevis* oocytes and displays a high potency and efficacy towards para/tipE. HNTX-I seems to act most likely as a site 1 antagonist, affecting the VGSCs through a mechanism quite similar to that of TTX. Thus the characterization of HNTX-I and the investigation of its interaction with VGSCs are very interesting. Given that HNTX-I targets both insect and mammalian VGSCs, it possesses a considerable potential as a pharmacological tool for aiding in the investigation of structural requirements for anti-insect versus anti-mammal activity. In addition, the primary sequence and structural details of the depressant toxin reported here provide further information not only concerning structure–function relationship but also regarding the design of genetic or synthetic analogs for future functional studies.

References

[1] Catterall, W.A. (2000) Neuron 26, 13–25.
[2] Stevens, E.B., Cox, P.J., Shah, B.S., Dixon, A.K., Richardson, P.J., Pinnock, R.D. and Lee, K. (2001) Eur. J. Physiol. 441, 481–488.
[3] Goldin, A.L., Barchi, R.L., Caldwell, J.H., Hofmann, F., Howe, J.R., Hunter, J.C., Kallen, R.G., Mandel, G., Meisler, M.H. and Berwald, N. et al. (2000) Neuron 28, 365–368.
[4] Lopreato, G.F., Lu, Y., Southwell, A., Athinson, N.S., Hillis, D.M., Wilcox, T.P. and Zakon, H. (2001) Proc. Natl. Acad. Sci. USA 98, 7588–7592.
[5] Goldin, A.L. (2002) J. Exp. Biol. 205, 575–584.

[6] Wicher, D., Walther, C. and Wicher, C. (2001) Prog. Neurobiol. 64, 431–525.

[7] Wicher, D. and Penzlin, H. (1998) Receptors Channels 5, 355–366.

[8] Cestèle, S. and Catterall, W.A. (2000) Biochimie 82, 883–892.

[9] Liu, Z.H., Dai, J., Chen, Z.R., Hu, W.J., Xiao, Y.C. and Liang, S.P. (2003) Cell. Mol. Life Sci. 60, 972–978.

[10] Peng, K., Shu, Q., Liu, Z.H. and Liang, S.P. (2002) J. Biol. Chem. 277, 47564–47571.

[11] Omecinsky, D.O., Holub, K.E., Adams, M.E. and Reily, M.D. (1996) Biochemistry 35, 2836–2844.

[12] Escoubas, P., Diochot, S. and Corzo, G. (2000) Biochimie 82, 893–907.

[13] Fletcher, J.I., Chapman, B.E., Mackay, J.P., Howden, M.E. and King, G.F. (1997) Structure 5, 1525–1535.

[14] Szeto, T.H., Birinyi-Strachan, L.C., Smith, R., Connor, M., Christie, M.J., King, G.F. and Nicholson, G.M. (2000) FEBS Lett. 470, 293–299.

[15] Nicholson, G.M. and Graudins, A. (2002) Clin. Exp. Pharmacol. Physiol. 29, 785–794.

[16] Gilles, N., Harrison, G., Karbat, I., Gurevitz, M., Nicholson, G.M. and Gordon, D. (2002) Eur. J. Biochem. 269, 1500–1510.

[17] Liang, S.P., Peng, X.J. and Huang, R.H. (1999) Life Sci. Res. 3, 299–303.

[18] Xiao, Y.C. and Liang, S.P. (2003) Toxicon 41, 643–650.

[19] Pallaghy, P.K., Nielsen, K.J., Craik, D.J. and Norton, R.S. (1994) Protein Sci. 3, 1833–1839.

[20] Souslova, V.A., Fox, M., Wood, J.N. and Akopian, A.N. (1997) Genomics 41, 201–209.

[21] Warmke, J.W., Reenan, R.A.G., Wang, P., Qian, S., Arena, J.P., Wang, J., Wunderler, D., Liu, K., Kaczorowski, J.P. and Van Der Ploeg, L.H.T. et al. (1997) J. Gen. Physiol. 110, 119–133.

[22] Feng, G., Deák, P., Chopra, M. and Hall, L. (1995) Cell 82, 1001–1011.

[23] Noda, M., Ikeda, T., Kayano, T., Suzuki, H., Takeshima, H., Kurasaki, M., Takahashi, H. and Numa, S. (1986) Nature 320, 188–192.

[24] Gellens, M.E., George Jr., A.L., Chen, L.Q., Chahine, M., Horn, R., Barchi, R.L. and Kallen, R.G. (1992) Proc. Natl. Acad. Sci. USA 89, 554–558.

[25] Liman, E.R., Tytgat, J. and Hess, P. (1992) Neuron 9, 861–871.

[26] Wüthrich, K. (1986) NMR of Proteins and Nucleic Acids, John Wiley and Sons, New York.

[27] Brünger, A.T. (1992) X-PLOR manual, version 3.1, Yale University, New Haven, CT.

[28] Li, D.L. and Liang, S.P. (2003) Acta Biophys. Sin. (in press).

[29] Richardson, J.S. (1981) Adv. Protein Chem. 34, 167–339.

[30] Xiao, Y.C. and Liang, S.P. (2003) Eur. J. Pharmacol. 477, 1–7.

[31] Ma, B.Y., Elkayam, T., Wolfson, H. and Nussinov, R. (2003) Proc. Natl. Acad. Sci. USA 100, 5772–5777.

[32] Terlau, H., Heinemann, S.H., Stühmer, W., Pusch, M., Conti, F., Imoto, K. and Numa, S. (1991) FEBS Lett. 293, 93–96.

[33] Wakamatsu, K., Kohda, D., Hatanaka, H., Lancelin, J.M., Ishida, Y., Oya, M., Nakamura, H., Inagaki, F. and Sato, K. (1992) Biochemistry 31, 12577–12584.

[34] Cummins, T.R., Aglieco, F. and Dib-Hajj, S.D. (2002) Mol. Pharmacol. 61, 1192–1201.

[35] Hui, K., Lipkind, G., Fozzard, H.A. and French, R.J. (2002) J. Gen. Physiol. 119, 45–54.

[36] Li, R.A., Sato, K., Kodama, K., Kohno, T., Xue, T., Tomaselli, G.F. and Marbán, E. (2002) FEBS Lett. 511, 159–164.

[37] Yu, F.H. and Catterall, W.A. (2003) Genome Biol. 4, 207.1–207.7.

[38] Peng, K., Chen, X.D. and Liang, S.P. (2001) Toxicon 39, 491–498.

[39] Qu, Y.X., Liang, S.P., Ding, J.Z., Liu, X.C., Zhang, R.J. and Gu, X.C. (1997) J. Protein Chem. 16, 565–574.